First-in-human study of the biodistribution and pharmacokinetics of 89Zr-CX-072, a novel immunopet tracer based on an anti–PD-L1 probody

de Ruijter, Laura Kist; Hooiveld-Noeken, Jahlisa S.; Giesen, Danique; Lub-De Hooge, Marjolijn N.; Kok, Iris C.; Brouwers, Adrienne H.; Elias, Sjoerd G.; Nguyen, Margaret T.L.; Lu, Hong; Gietema, Jourik A.

Published in:
Clinical Cancer Research

DOI:
10.1158/1078-0432.CCR-21-0453

Publication date:
2021

Published OnlineFirst July 12, 2021; DOI: 10.1158/1078-0432.CCR-21-0453

First-in-Human Study of the Biodistribution and Pharmacokinetics of ^{89}Zr-CX-072, a Novel Immunopet Tracer Based on an Anti–PD-L1 Probody

Laura Kist de Ruijter[1], Jahlisa S. Hooiveld-Noeken[1], Danique Giesen[1], Marjolijn N. Lub-de Hooge[2], Iris C. Kok[1], Adrienne H. Brouwers[3], Sjoerd G. Elias[4], Margaret T.L. Nguyen[5], Hong Lu[5], Jourik A. Gietema[1], Mathilde Jalving[1], Derk J.A. de Groot[1], Olga Vasiljeva[5], and Elisabeth G.E. de Vries[1]

ABSTRACT

Purpose: CX-072, a PD-L1–targeting Probody therapeutic, is engineered to be activated by tumor proteases that remove a masking peptide. To study effects on biodistribution and pharmacokinetics, we performed ^{89}Zr-CX-072 positron emission tomography (PET) imaging.

Experimental Design: Patients received ∼1 mg, 37 MBq ^{89}Zr-CX-072 plus 0, 4, or 9 mg unlabeled CX-072 and PET scans at days 2, 4, and 7. After that, treatment comprised 10 mg/kg CX-072 q2 weeks ($n = 7$) + 3 mg/kg ipilimumab q3w 4× ($n = 1$). Normal organ tracer uptake was expressed as standardized uptake value $(SUV)_{mean}$ and tumor uptake as SUV_{max}. PD-L1 expression was measured immunohistochemically in archival tumor tissue.

Results: Three of the eight patients included received 10-mg protein dose resulting in a blood pool mean $SUV_{mean} \pm$ SD of 4.27 ± 0.45 on day 4, indicating sufficient available tracer. Tumor uptake was highest at day 7, with a geometric mean SUV_{max} 5.89 ($n = 113$) and present in all patients. The median follow-up was 12 weeks (4–76+). One patient experienced stable disease and two patients a partial response. PD-L1 tumor expression was 90% in one patient and ≤1% in the other patients. Mean $SUV_{mean} \pm$ SD day 4 at 10 mg in the spleen was 8.56 ± 1.04, bone marrow 2.21 ± 0.46, and liver 4.97 ± 0.97. Four patients out of seven showed uptake in normal lymph nodes and Waldeyer's ring. The tracer was intact in the serum or plasma.

Conclusions: ^{89}Zr-CX-072 showed tumor uptake, even in lesions with ≤1% PD-L1 expression, and modest uptake in normal lymphoid organs, with no unexpected uptake in other healthy tissues.

Introduction

Immune-checkpoint inhibitors yield impressive responses in patients with locally advanced and metastatic malignancies and can result in long-term survival in a subset of cancer patients. Currently, ipilimumab targeting cytotoxic T lymphocyte-associated antigen 4 (CTLA-4) and several programmed cell death protein 1 (PD-1)– and PD-1 ligand 1 (PD-L1)–targeting medicines are registered for multiple tumor types. The antitumor efficacy of immune-checkpoint inhibitors is higher when combined, as seen for nivolumab plus ipilimumab (1–3). Immune-related toxicity is induced by all immune-checkpoint inhibitors. However, the percentage of patients with side effects increases from 20% for single immune-checkpoint inhibitors to 54% when ipilimumab and nivolumab are combined (4).

These immune-related toxicities have stimulated the development of medicines that have similar pharmacologic activity but fewer side effects. CX-072, a Probody therapeutic directed against PD-L1, is a prime example of this. This recombinant monoclonal antibody prodrug is designed to be conditionally activated by proteases in the tumor microenvironment. CX-072 contains a mask with a protease-cleavable substrate at the amino-terminus of the light chain. This mask is devised to block PD-L1 binding until it is released in the tumor microenvironment. The effect of such modifications on antibody biodistribution and kinetics is unknown.

Molecular imaging is increasingly seen as an approach to facilitate drug development (5). An antibody labeled to a positron emission tomography (PET) isotope, such as zirconium-89 (^{89}Zr), which complements the long biological half-life of antibodies, allows the collection of data on whole-body drug distribution (6, 7). PD-L1 is expressed by tumor cells, as well as by macrophages, dendritic cells, and T cells. Clinical PET imaging with ^{89}Zr-atezolizumab, a zirconium-labeled PD-L1 antibody, showed uptake in tumor lesions and the spleen, lymph nodes, Waldeyer's ring, and sites of inflammation (8). Whole-body PET imaging may also provide information as a biomarker. For example, higher ^{89}Zr-atezolizumab tumor uptake correlated with better tumor response and overall survival in cancer patients treated with atezolizumab (8), and uptake on ^{89}Zr-trastuzumab PET was predictive for effect of trastuzumab–emtansine therapy in patients with breast cancer (9).

In immune-competent mice, ^{89}Zr-CX-072 PET showed specific drug accumulation in PD-L1–expressing human tumors with minor uptake in lymphoid tissues (10). In patients with advanced solid tumors, long-term treatment with CX-072 administered as a single

[1]Department of Medical Oncology, University Medical Center Groningen, University of Groningen, Groningen, the Netherlands. [2]Department of Clinical Pharmacy and Pharmacology, University Medical Center Groningen, University of Groningen, Groningen, the Netherlands. [3]Medical Imaging Center, University Medical Center Groningen, University of Groningen, Groningen, the Netherlands. [4]Department of Epidemiology, Julius Center for Health Sciences and Primary Care, University Medical Center Utrecht, Utrecht University, Utrecht, the Netherlands. [5]CytomX Therapeutics Inc., South San Francisco, California.

Note: Supplementary data for this article are available at Clinical Cancer Research Online (http://clincancerres.aacrjournals.org/).

Corresponding Authors: Elisabeth G.E. de Vries, Department of Medical Oncology, University Medical Center Groningen, P.O. Box 30.001, 9700 RB Groningen, the Netherlands. Phone: 31503612821; Fax: 31503614862; E-mail: e.de.vries@umcg.nl; and Olga Vasiljeva, CytomX Therapeutics, Inc., 151 Oyster Point Boulevard, South San Francisco, CA 94080. Phone: 650-515-3912; E-mail: ovasiljeva@cytomx.com

Clin Cancer Res 2021;27:5325–33

doi: 10.1158/1078-0432.CCR-21-0453

Published OnlineFirst July 12, 2021; DOI: 10.1158/1078-0432.CCR-21-0453

Translational Relevance

The PD-L1–targeting antibody CX-072 is engineered to be conditionally activated in the tumor microenvironment by tumor-associated proteases and to remain predominantly masked in the circulation. This has raised interest in the effects of this design on biodistribution and pharmacokinetics. Therefore, we performed whole-body ^{89}Zr-CX-072 PET imaging in patients. ^{89}Zr-CX-072 showed evident tumor uptake, even in lesions with ≤1% PD-L1 expression in tumor biopsies, modest uptake in normal lymphoid organs, and no unexpected uptake in other healthy tissues. The highest normal tissue uptake was in the spleen, although less than the nonconditionally activated ^{89}Zr-labeled PD-L1 antibody ^{89}Zr-atezolizumab. ^{89}Zr-CX-072 was found to be intact in the circulation, predominantly in its masked form. Our findings indicate that ^{89}Zr-CX-072 PET provides insight into the whole-body distribution of a newly designed therapeutic drug candidate that can be achieved with a small number of patients.

agent or in combination with ipilimumab has shown durable objective responses in patients with advanced solid tumors (11, 12).

We aimed to obtain insight into CX-072 biodistribution and pharmacokinetics (PK) and to learn whether CX-072's Probody therapeutic design influences them. Therefore, we studied ^{89}Zr-CX-072 biodistribution in patients with locally advanced or metastatic malignancies.

Materials and Methods

Study design and participants

This is a single-center, prospective substudy of an international multicenter phase I–II treatment study. Eligible patients had measurable advanced or metastatic solid malignancies, archival tumor tissue available, age >18 years, Eastern Cooperative Oncology Group performance status (ECOG PS) of 0–1, an anticipated life expectancy of at least 3 months, and stable hematologic and chemistry laboratory values. The main study and the substudy were approved by the medical ethical committee of the University Medical Center Groningen (UMCG). PD-L1 expression in the tumor was not required for eligibility to the substudy. All patients gave written informed consent. The study is registered in ClinicalTrials.gov (NCT03013491).

Procedures

Patient screening was performed within 30 days before tracer injection and comprised a baseline computed tomography (CT), electrocardiogram (ECG), and laboratory assessment. After completing the imaging substudy part, patients received CX-072 at their assigned dose cohort 10 mg/kg every 2 weeks, with or without an initial combination with 4 cycles of ipilimumab given at 3 mg/kg at 3 weekly intervals. Treatment with CX-072 was initiated within 10 days after the last PET scan.

Tumor response was assessed every 8 weeks and after one year every 12 weeks. The objective response was defined as a complete or partial response on two consecutive tumor assessments at least 4 weeks apart, according to RECIST version 1.1 and irRECIST (13, 14).

PD-L1 expression in archival tissue biopsies, performed at the latest 27 months before the study start, was determined by PD-L1 immunohistochemistry (IHC) 22C3 pharmDx assay (Dako) and scored as the percentage of viable tumor cells showing partial or complete membrane staining of PD-L1.

Tracer development and PET imaging

Clinical-grade ^{89}Zr-CX-072 was developed and produced in the UMCG, as described previously (10). For quality control, ^{89}Zr-CX-072 met all release specifications on conjugation ratio, radioactive yield, protein purity, concentration, pH, radiochemical purity, residual solvents, sterility, and endotoxin content. Preservation of immunoreactivity after conjugation was verified by enzyme-linked immunosorbent assay (ELISA).

Cohorts of 2 to 3 patients received 37 MBq of ∼1 mg ^{89}Zr-CX-072 plus 0 mg, 4 mg, or 9 mg unlabeled CX-072 (∼1 mg, 5 mg, or 10 mg total tracer protein doses) until sufficient blood pool levels were reached with satisfactory visualization of tumor lesions. Sufficient unlabeled dose supplementation was determined by comparing ^{89}Zr-CX-072 SUV_{mean} in the blood pool at day 4 with other ^{89}Zr antibody tracers with well-known kinetics over time (9, 15, 16), thereby taking into account deposition in sink organs known for a PD-L1 antibody (8).

^{89}Zr-CX-072 safety was assessed through changes in laboratory test results, changes in vital signs, and summaries of adverse events (AE) before and after exposure to ^{89}Zr-CX-072. AE data were recorded according to NCI Common Terminology Criteria for Adverse Events v4.0.

All PET scans were performed on days 2, 4, and 7 after tracer administration and combined with a low-dose CT scan for attenuation correction and anatomic reference, on a Siemens Biograph mCT 40 or 64-slice PET/CT camera, as described previously (8). PET images were reconstructed with the parameters advised for multicenter ^{89}Zr-monoclonal antibody PET scan trials, according to EARL1 (17).

Biodistribution and tumor lesion quantification

Quantification of tracer uptake in normal tissues and tumor lesions was performed in the ACCURATE tool by manually placing a 3D-sphere as the volume of interest (VOI) on each of the three post tracer administration PET scans for each patient (18) (RRID: SCR_020955). Tumor lesions were identified before treatment by conventional imaging techniques according to RECIST1.1. Standardized uptake value (SUV) was calculated using net injected dose, body weight, and measured radioactivity within the VOI on the PET image, corrected for decay. The tracer uptake in healthy tissue was expressed as mean standardized uptake value (SUV_{mean}; average uptake within a VOI), which is standard for calculating physiologic uptake in homogeneous tissues. SUV_{mean} is reported with ± standard deviation. In tumor lesions, uptake was calculated as maximum SUV (SUV_{max}; maximum uptake within a VOI) to assess target-specific uptake.

Uptake of ^{89}Zr-CX-072 in Waldeyer's ring, axillary, and inguinal lymph nodes was assessed visually. The uptake was compared to the background as well as liver and spleen.

Plasma PK and ADA assay

Blood samples for PK analysis were obtained at 30 minutes and on days 2, 4, and 7 after tracer administration.

Magnetic beads coated with protein A were used to enrich for immunoglobulin (including intact and cleaved CX-072) in K2EDTA plasma samples. Following protein denaturation, reduction, and alkylation, the proteins were digested with trypsin, and two peptide fragments to CX-072 were monitored: 1 peptide from the CX-072 heavy chain present in both the intact and active forms of CX-072 (for quantitation of total CX-072) and 1 peptide from the CX-072 prodomain present only in the intact form of CX-072 (for quantitation of intact CX-072). Corresponding stable isotope-labeled peptides were used as internal standards. The final extract was analyzed via

Published OnlineFirst July 12, 2021; DOI: 10.1158/1078-0432.CCR-21-0453

high-performance liquid chromatography mass spectrometry with tandem mass spectrometry detection using positive ion electrospray. The assay has a quantifiable range of 0.657 to 328 nmol/L for intact and total CX-072.

Blood samples were obtained before tracer infusion to study the presence of endogenous anti-drug antibodies (ADA) against CX-072. A validated method using solid-phase extraction with acid dissociation (SPEAD) sample pretreatment followed by a direct electrochemiluminescent assay was used to detect anti-CX-072 antibodies in serum. To maximize the detection of ADAs to CX-072, including antibodies directed against the target binding region, ADAs were extracted from serum using a 1:1 mixture of biotinylated CX-072 and biotinylated CX-075 (parental antibody of CX-072). Following SPEAD processing steps, anti-CX-072 antibodies were detected using a 1:1 mixture of sulfo-tagged CX-072 and sulfo-tagged CX-075. Sample testing was conducted in a tiered manner beginning with a screening assay, which identified presumptive positive or negative samples. This was followed by confirmatory assays. The screening sensitivity is 2.72 ng/mL.

Tracer integrity

The intactness of the ^{89}Zr-CX-072 was studied in serum or plasma, depending on sample availability, collected days 2, 4, and 7 with sodium dodecyl sulfate-polyacrylamide gel electrophoresis (SDS-PAGE) as described previously (10). To detect a ±4 kDa difference between masked and unmasked antibody, ^{89}Zr-CX-072 was reduced to its heavy and light chains using β-mercaptoethanol. Intact ^{89}Zr-CX-072 was used as control and diluted to match sample radioactivity. ^{89}Zr-CX-072 was detected autoradiographically by exposing gels to a multipurpose phosphor plate (PerkinElmer) overnight at −20°C. Exposures were captured using a Cyclone phosphor imager. Intact tracer and masked versus unmasked antibody were quantified using ImageJ (version 1.52p, RRID: SCR_003070).

Statistical analysis

Descriptive statistics (i.e., mean and SDs), median counts, and percentages were used to provide an overview of the patient population and ^{89}Zr-CX-072 uptake values. Despite the early-phase nature of this study (without *a priori*–defined testable hypotheses and supporting sample size calculations), and the limited number of patients studied, we performed various exploratory statistical analyses making optimal use of the wealth of repeated measurements that are obtainable using PET imaging in patients with metastatic cancer. To describe the ^{89}Zr-CX-072 biodistribution according to administered dose and time post-tracer administration in terms of tumor uptake, we used linear mixed models. The natural logarithmic of the SUV_{max} was used as dependent variable (to account for its right-skewed distribution), taking within-patient and within-tumor clustering into account using nested random intercepts. The results of these models are expressed as geometric mean uptake levels. To allow post-injection time–tumor–uptake patterns to be variable between dose groups, interaction terms between days post-injection and dose were added to the models. They were tested for statistical significance using the likelihood ratio test under maximum likelihood (such tests also served to test the contribution of other variables to tumor uptake). Besides analyzing days post-tracer administration as a categorical variable, it was also analyzed continuously, choosing the best-fitting form from a linear, a log-linear, or a quadratic curve using the Akaike's Information Criterion under maximum likelihood. The ^{89}Zr-CX-072 biodistribution in normal tissues was assessed using similar linear mixed-effect models using SUV_{mean} as the dependent variable, for which a natural logarithmic (or other) transformation was not necessary.

Again, as strictly exploratory, the relation between best treatment response per patient and tumor uptake was analyzed by similar linear mixed-effect models. The relation between geometric mean tumor SUV_{max} per patient at day 7 post-injection and overall survival was studied using Firth's penalized maximum likelihood small-sample bias reduction method for Cox regression and assuming linearity and proportionality. All reported statistical tests are two-sided, without correction for multiple testing. Main analyses were performed using R version 3.2.1 for macOS, particularly using packages lme4 (1.1-11, RRID: SCR_015654), lmerTest (2.0-20, RRID: SCR_015656), and coxphf (1.11).

Results

Eight patients were enrolled between March 2018 and November 2018. Patient characteristics are listed in **Table 1**. All patients completed the entire PET scan series, and none experienced tracer-related AEs. Two patients received a total protein dose of 1 mg, three patients 5 mg, and three patients 10 mg. Thereafter treatment consisted of CX-072 monotherapy, and one patient additionally received ipilimumab (Supplementary Table S2).

^{89}Zr-CX-072 uptake in tumor lesions

In total, 118 tumor lesions were identified, of which 5 were not included in the following analyses as these were irradiated within

Table 1. Patient and tumor characteristics.

Characteristics	*n* = 8
Age, median (range), years	56 (40–68)
Sex, *n* (%)	
Male	3 (37.5)
Female	5 (62.5)
Primary tumor, *n* (%)	
MSI-high colorectal carcinoma	3 (37.5)
Pancreatic carcinoma	1 (12.5)
Ovarian carcinoma	1 (12.5)
Cervical carcinoma	1 (12.5)
Anaplastic thyroid carcinoma	1 (12.5)
Germ cell tumor	1 (12.5)
ECOG PS, *n* (%)	
0	4 (50)
1	4 (50)
Prior lines of therapy, *n* (%)	
0	1 (12.5)
1	1 (12.5)
≥ 2	6 (75)
Tumor lesion sites, *n* (%)	
Total number lesions	118 (100)
Lung	36 (30.5)
Lymph node	36 (30.5)
Soft tissue	27 (21.6)
Liver	8 (6.8)
Bone	4 (3.4)
Pancreas	2 (1.7)
Spleen	2 (1.7)
Intestine	1 (0.8)
Kidney	1 (0.8)
Thyroid	1 (0.8)
IHC tumor PD-L1, *n* (%)	
≤1%	7 (87.5)
90%	1 (12.5)

Published OnlineFirst July 12, 2021; DOI: 10.1158/1078-0432.CCR-21-0453

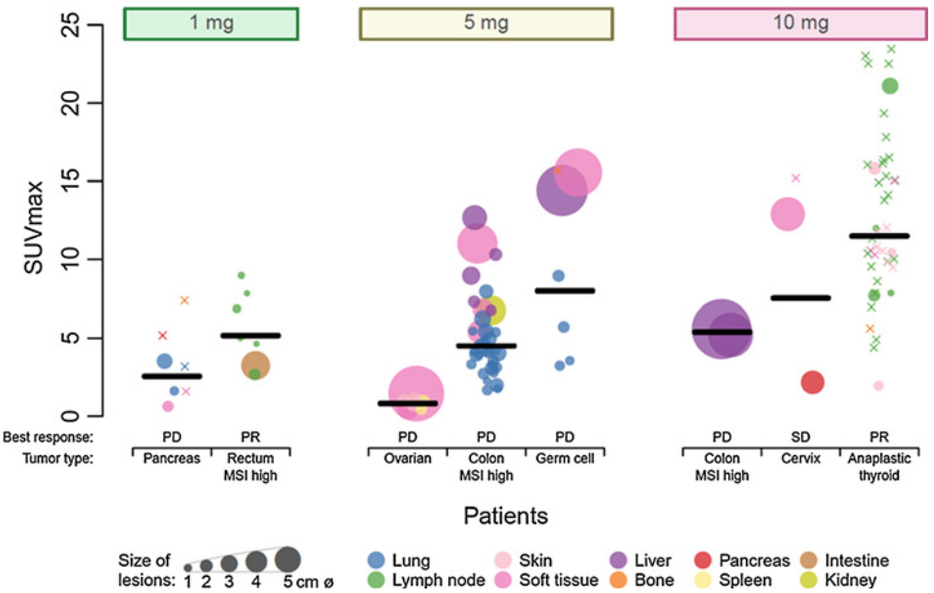

Figure 1.
SUV_{max} ^{89}Zr-CX-072 for the 113 tumor lesions of the eight patients for the three different tracer protein doses indicated by the color bars at the top; 1 mg ($n = 2$), 5 mg ($n = 3$), and 10 mg ($n = 3$). The geometric mean SUV_{max} of all lesions within a patient is indicated by the black horizontal line. A single lesion is marked with either a dot or "×" in case of an unmeasurable lesion. The dots' size corresponds with the anatomic size of the lesion and the color with the location of the lesion. Best responses are mentioned on the *x* axis above tumor type.

3–12 weeks before tracer injection. Tumor characteristics, best response, and the geometric mean of SUV_{max} per patient at day 7 post-injection are shown in **Fig. 1**.

Tumor uptake was heterogeneous within and between patients. The highest tumor lesion uptake and the highest geometric mean of SUV_{max} per patient were seen at the 10-mg dose. All patients showed uptake in their tumor lesions, with an overall geometric mean SUV_{max} of 4.73 (95% CI: 2.81–7.94; averaged over day 2–7 post-injection). Tumor uptake at 10-mg dose increased between day 2–7 post-injection, but not at other dose levels (**Fig. 2**). Of the 113 nonirradiated lesions defined by conventional imaging techniques, 84 were visually detected by conventional imaging and by ^{89}Zr-CX-072 PET. These

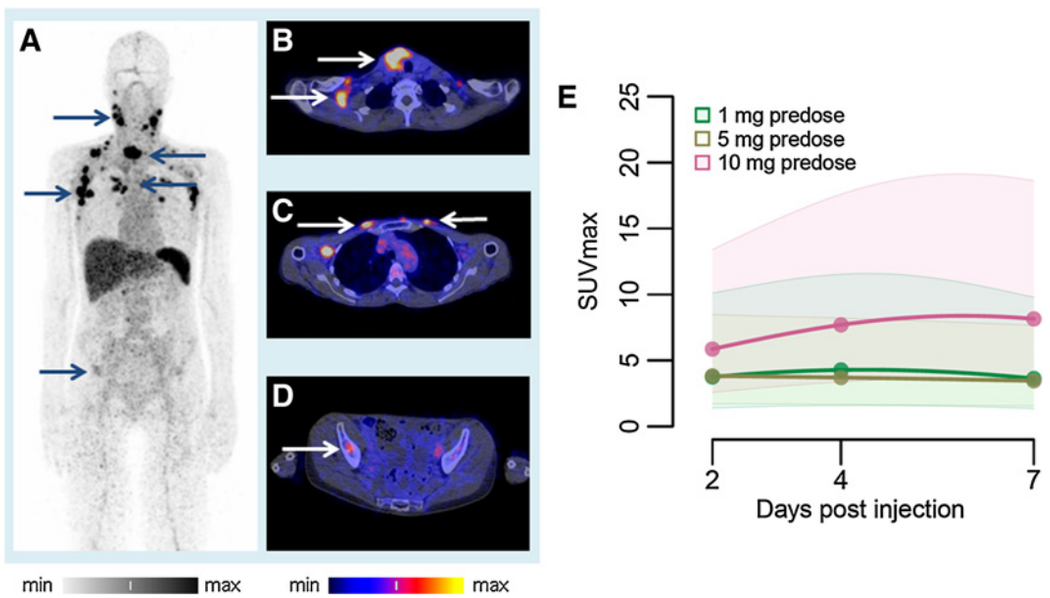

Figure 2.
Uptake of ^{89}Zr-CX-072 in tumor lesions. **A,** Maximum intensity projection of ^{89}Zr-CX-072 PET on day 7 post-injection in a patient with anaplastic thyroid cancer with 10-mg total protein dose. Arrows show uptake in a thyroid tumor mass, cutaneous tumor lesions on the chest, malignant lymph nodes in the neck and axilla, and a bone lesion in the pelvis. **B,** Axial view of ^{89}Zr-CX-072 PET-CT shows uptake in thyroid mass and malignant lymph nodes. **C,** Axial view of ^{89}Zr-CX-072 PET-CT shows uptake in cutaneous lesions on the chest and malignant axillary lymph nodes. **D,** Axial view of ^{89}Zr-CX-072 PET-CT shows uptake in a pelvic bone lesion. **E,** SUV_{max} ^{89}Zr-CX-072 tumor uptake per tracer protein dose. Tumor uptake is highest at 10 mg (albeit nonsignificantly: likelihood ratio test for effect of dose on uptake $P = 0.25$). Between days 2 and 7, the uptake increases in the 10-mg protein group, whereas the uptake stays stable in the other dose groups (likelihood ratio test for interaction for a different time-tumor–uptake pattern across dose groups $P = 0.000044$).

Published OnlineFirst July 12, 2021; DOI: 10.1158/1078-0432.CCR-21-0453

included lymph nodes with a short axis of less than 1.5 cm but defined as malignant based on other clinical or CT features, and 5 skin lesions not visible on CT. At the same time, 28 lesions were not distinguishable from the background or did not show uptake by ^{89}Zr-CX-072 PET, but were detectable by conventional imaging techniques. One lesion was visible on ^{89}Zr-CX-072 PET that was not visible on CT imaging at baseline, but appeared malignant on the CT 6 weeks later.

The median follow-up at data cutoff on November 7, 2020, is 12 weeks (range, 4–76+). One patient experienced stable disease (SD) and two a partial response (PR). The geometric mean SUV_{max} in tumor lesions from patients with at least stable disease as best response was 6.84 (95% CI: 2.25–20.78; 3 patients with 52 lesions) and was 3.62 (95% CI: 1.57–8.36; 5 patients with 61 lesions) in patients with progressive disease (PD) (likelihood ratio $P = 0.14$; averaged over day 2–7 post-injection and adjusted for differences in administered dose between patients). The patient with anaplastic thyroid cancer who experienced a PR for 18 months had high ^{89}Zr-CX-072 tumor uptake with geometric mean SUV_{max} 11.49 (**Figs. 1** and **2**). Furthermore, a patient with microsatellite instable (MSI) high colorectal cancer who responded as well showed uptake in an irresectable sacral local recurrence with SUV_{max} 3.25 on day 7 (blood pool day 7 at 1 mg mean SUV_{mean} 1.65), lacking expression of PD-L1 by IHC. This tumor became resectable and was surgically removed after 15 months of treatment. At data cutoff, this patient was free of disease for 11 months. In an exploratory univariable survival analysis accounting for small sample bias (8 patients, 6 events), the hazard ratio for dying was estimated to be 1.32 (95% CI: 0.98–1.93) per unit decrease in per-patient geometric mean tumor SUV_{max} (likelihood ratio $P = 0.070$). PD-L1 tumor expression measured immunohistochemically was 90% in the patient with anaplastic thyroid tumor, in the other patients this was ≤1%.

Biodistribution and pharmacokinetics of ^{89}Zr-CX-072

The mean SUV_{mean} in the blood pool at the 10-mg protein dose on day 4 was 4.27 ± 0.45, indicating sufficient tracer levels available to reach tumor lesions. At this dose, the mean SUV_{mean} at day 4 in the liver was 5.05 ± 0.75 and the kidney 2.71 ± 0.64. **Figure 3** shows the SUV_{mean} for days 2, 4, and 7 after tracer injection with 1-, 5-, and 10-mg protein dose across the normal tissues.

Remarkable was the spleen SUV_{mean}, which was the highest of all healthy organs. Corrected for decay at each time point, the SUV_{mean} of the spleen was highest at 1 mg ($n = 2$), lower at 5 mg ($n = 3$), and the lowest at 10 mg ($n = 3$) (test for effect of dose on uptake: likelihood ratio $P = 0.017$). In the liver, the average SUV_{mean} also lowered with increasing tracer protein doses. The spleen uptake was already high on day 2; however, in contrast to what was seen in the tumor lesions, it did not further increase the days thereafter. In both spleen and liver, uptake was stable over time. In other healthy parenchymal tissues, the PET signal decreased over the days after tracer injection.

The bone marrow mean SUV_{mean} at 10 mg was 2.54 ± 0.49 and remained stable over time. We also studied ^{89}Zr-CX-072 uptake in other lymphoid tissues. The ^{89}Zr-CX-072 uptake in the Waldeyer's ring on day 7 was present in four patients. Uptake of ^{89}Zr-CX-072 was present on day 7, in axillary lymph nodes in four

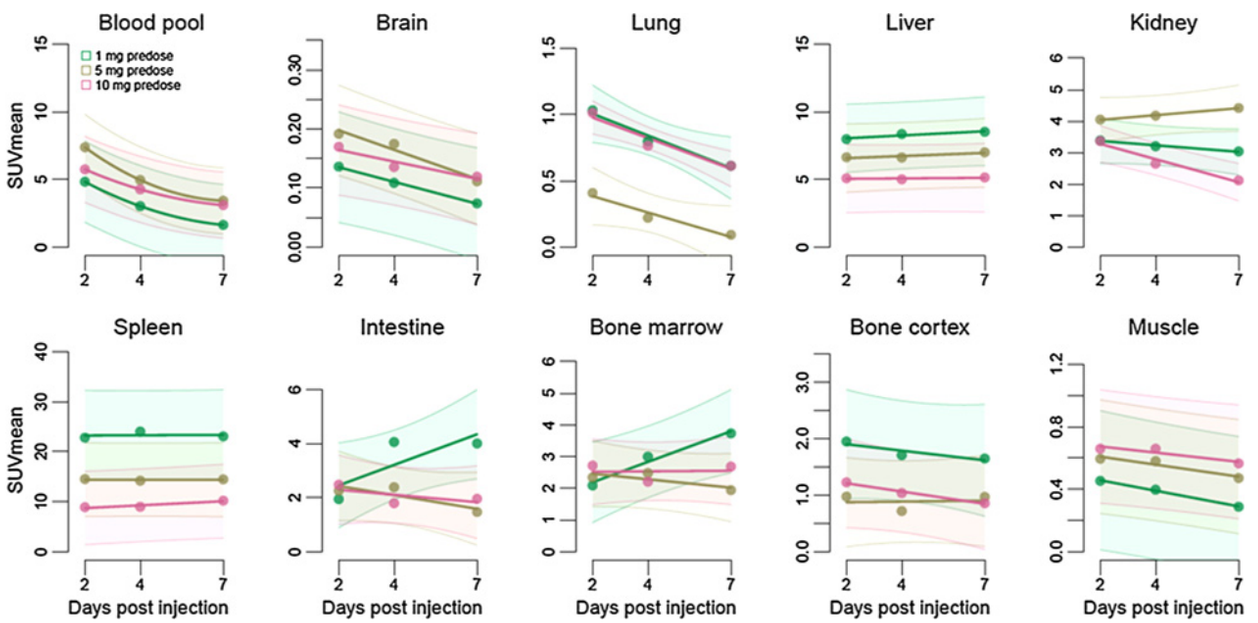

Figure 3.
Uptake in ^{89}Zr-CX-072 in normal tissues per tracer protein dose. SUV_{mean} days 2, 4, and 7 after tracer injection with 1-, 5-, and 10-mg protein dose in blood pool, brain, lung, liver, kidney, spleen, intestine, bone marrow, bone cortex, and muscle. SUV_{mean} ^{89}Zr-CX-072 in the spleen shows the lowest uptake at 10-mg protein dose (likelihood ratio test for effect of dose on uptake: $P = 0.017$). Uptake in the spleen stays stable over time (likelihood ratio test for a different time–spleen–uptake pattern across dose groups: $P = 0.54$). Fitted regression lines with 95% CI are based on linear mixed-effect models taking clustering within patients (and for spleen and liver uptake multiple regions) into account.

Published OnlineFirst July 12, 2021; DOI: 10.1158/1078-0432.CCR-21-0453

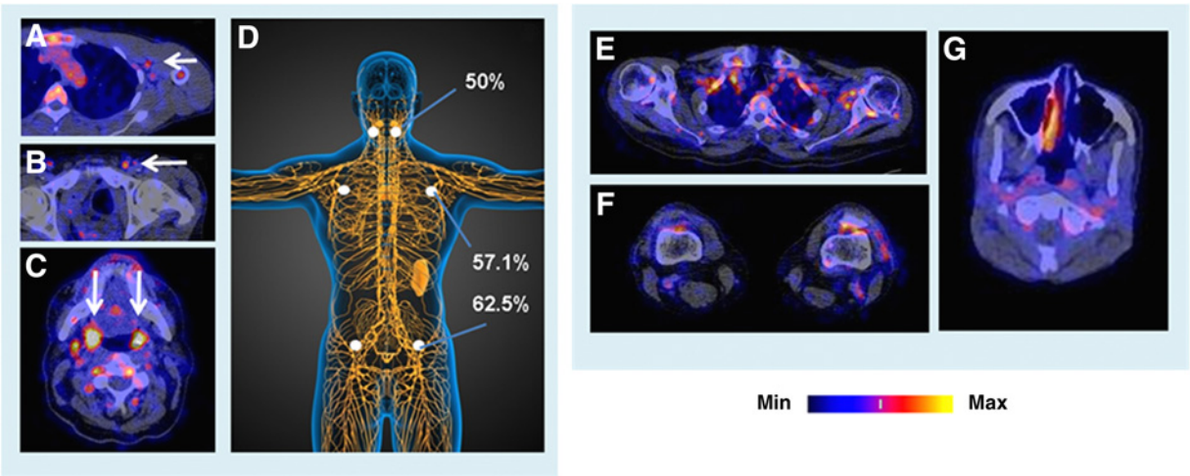

Figure 4.

Uptake of ^{89}Zr-CX-072 in lymphoid tissues and sites of inflammation. Top, examples of visual moderate to clear ^{89}Zr-CX-072 PET-CT uptake in lymphoid tissues on day 7 post-injection. **A,** Axial view of the left axilla region with uptake in lymph nodes. **B,** Axial view of the inguinal region with uptake in inguinal lymph nodes. **C,** Axial view of Waldeyer's ring region with high uptake in tonsils. **D,** Percentages of patients with visual uptake on day 7 of different lymphoid tissue stations: tonsils ($n = 8$), axillary lymph nodes ($n = 7$), and inguinal lymph nodes ($n = 8$). Bottom, examples of ^{89}Zr-CX-072 PET-CT of sites of inflammation. **E,** Patient with polyarthritis and uptake in left shoulder and (**F**) knee joints. **G,** Other patient with unilateral rhinosinusitis.

out of seven patients, and in inguinal lymph nodes in five out of eight patients. Percentages of visual uptake in Waldeyer's ring and lymph nodes are shown in **Fig. 4**. Visual uptake did not differ between tracer protein doses and occurred at all doses (Supplementary Table S1).

^{89}Zr-CX-072 uptake in sites of inflammation

^{89}Zr-CX-072 uptake was also observed at sites of inflammation in two patients: one with polyarthritis and another with unilateral rhinosinusitis (**Fig. 4**).

Pharmacokinetic analysis

Intact and total CX-072 protein concentrations at evaluated time plots for subjects receiving a total dose of 10 mg are depicted in **Fig. 5B**. Notably, CX-072 concentration was below the limit of quantitation (LQ) in 32% of all PK samples and corresponded to those patients who received 1- and 5-mg doses. Following the 10-mg dose, intact and total CX-072 concentrations remained above the LQ for PK sampling duration. Measurement of ^{89}Zr blood radioactivity was not performed. All subjects were ADA negative at baseline.

Tracer integrity and degree of unactivated CX-072

^{89}Zr-CX-072 integrity in blood samples collected up to 7 days after injection in five patients showed intactness of ^{89}Zr-bound CX-072. CX-072 was predominantly present in its masked, unactivated form, up to day 7 (**Fig. 5B–E**).

Discussion

This is the first-in-human study with ^{89}Zr-labeled Probody therapeutic PET imaging to study CX-072 drug biodistribution. We showed clear ^{89}Zr-CX-072 tumor uptake in all patients, even in lesions of patients lacking IHC PD-L1 tumor expression. There was modest uptake in normal lymphoid organs without unexpected uptake in other healthy tissues.

The rationale behind the Probody therapeutic design is that the molecule is conditionally activated in the tumor. This should reduce the distribution of its activated form in normal tissues compared with current, unmodified, PD-L1 antibodies, while drug uptake in tumor lesions is not affected. In immune-competent mice, ^{89}Zr-CX-072 PET did indeed show drug accumulation in PD-L1 expressing human tumors similar to the parental antibody and minor uptake in lymphoid tissues (10). Our current study with ^{89}Zr-CX-072 PET allowed further analysis of these properties in humans. We have shown that ^{89}Zr-CX-072 was intact in the blood for up to 7 days and predominantly in its masked form in circulation, consistent with Probody therapeutic design and in agreement with findings from the PK analyses from the treatment studies (19). CX-072 shows a linear PK in doses that are comparable to the used tracer proteins doses in this imaging study (19), so the biodistribution of the tracer is representative for CX-072 in therapeutic dose.

All patients showed ^{89}Zr-CX-072 uptake into tumor lesions. At 10 mg, uptake in tumor lesions increased between days 2 and 7. *In vitro* studies have priorly shown ^{89}Zr-CX-072 bound to PD-L1 on tumor cells can internalize, followed by intracellular residualization of radioactivity (10). In the current imaging study, at all doses, the tumor-to-blood ratio increased over time and was highest in the 10-mg cohort. Normal healthy organs without target show nonspecific ^{89}Zr-CX-072 uptake on the PET scan, which lowers with decreasing blood pool activity. Therefore, increasing ^{89}Zr-CX-072 uptake in tumor lesions over time suggests that this tumor uptake is specific and that ^{89}Zr-CX-072 is retained in the tumor by its interaction with PD-L1.

Tumor uptake was heterogeneous within and between patients. Also, ^{89}Zr-CX-072 tumor uptake was seen in patients whose tumors had low PD-L1 expression by IHC on archival tissue. The same was the case in the ^{89}Zr-atezolizumab PET imaging study, in which a biopsy was performed immediately after the last PET scan (8). The ^{89}Zr-atezolizumab tumor uptake into that specific biopsied lesion was also seen when PD-L1 staining was negative.

Tumor tracer uptake showed target-mediated, specific kinetics. Therefore, this discrepancy may be explained by heterogeneous

Published OnlineFirst July 12, 2021; DOI: 10.1158/1078-0432.CCR-21-0453

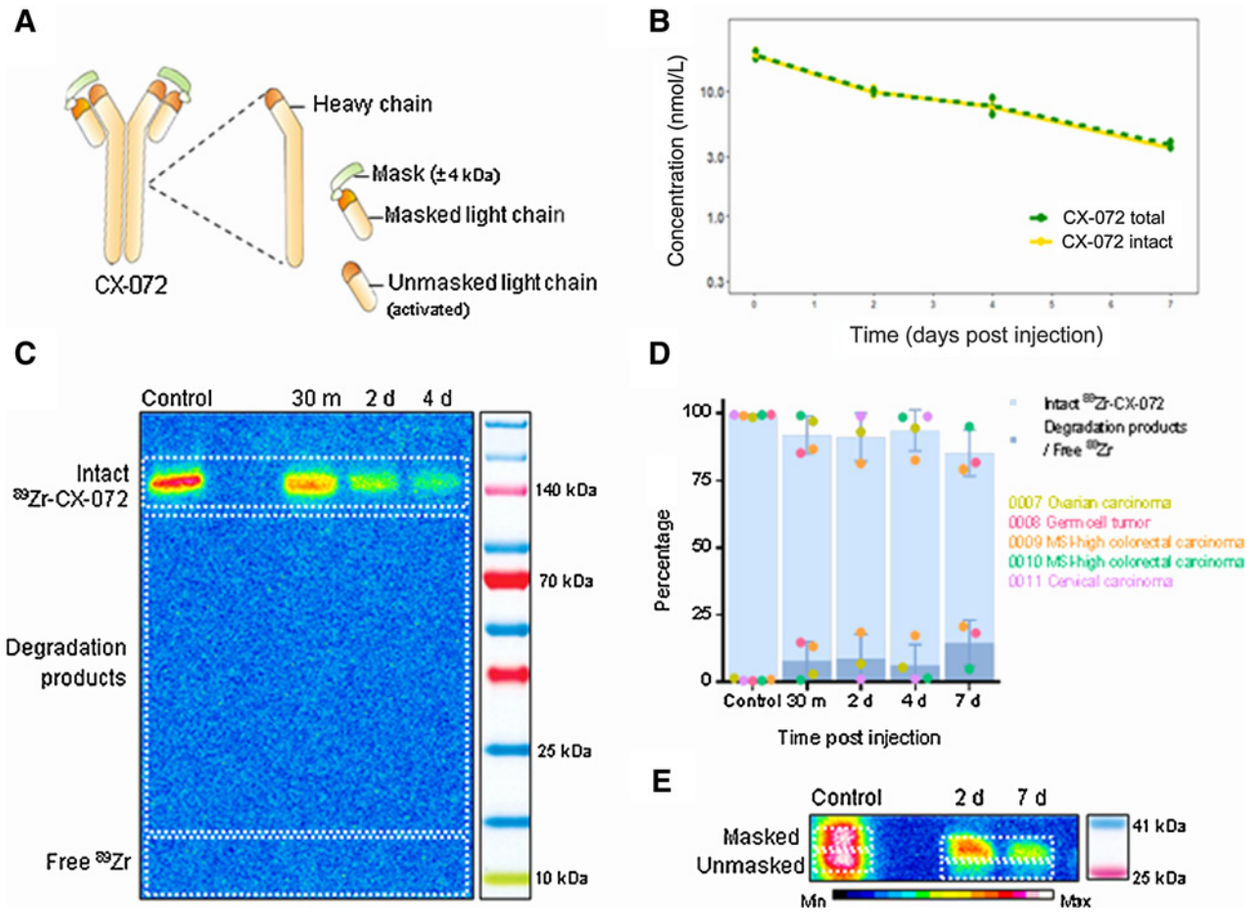

Figure 5.

Pharmacokinetic analysis, tracer integrity, and assessment of CX-072 activation. **A,** Schematic structure of CX-072 heavy- and light-chain variants. **B,** Intact and total CX-072 concentration versus time for subjects received 10 mg tracer protein dose ($n = 3$). **C,** Representative example of *ex vivo* serum or plasma SDS-PAGE analysis, ^{89}Zr-CX-072 remained intact up to 7 days. **D,** Quantification of intact tracer in samples obtained from $n = 5$ patients at 30 minutes and 2, 4, and 7 days after tracer administration. **E,** After reducing ^{89}Zr-CX-072 to its heavy and light chains, SDS-PAGE showed ^{89}Zr-CX-072 is predominantly present in its masked form up to 7 days. Intact ^{89}Zr-CX-072 was used as control.

PD-L1 expression within one tumor lesion, where tissue analysis is limited when taking only a small biopsy (20). Also, heterogeneity for PD-L1 expression between archival tissue material and current metastases may play a role. Moreover, PD-L1 expression by tumor cells is dynamic, causing temporal differences (20). Therefore, molecular imaging with a tracer that internalizes, including ^{89}Zr-CX-072, may provide an accumulated image of target expression over time. In contrast, IHC shows target expression at a given time point and could miss this dynamic expression. Finally, as molecular imaging shows target expression in the total lesion and in the whole body, it overcomes biases on sampling and heterogeneity between and within tumor lesions.

^{89}Zr-CX-072 tumor uptake was highest for the 10-mg dose, although the high PD-L1 expression in one patient may have played a role in this. Exploratory analyses suggest a positive association between uptake and patient outcome, corroborating our previous findings in the ^{89}Zr-atezolizumab PET imaging study. However, the number of patients is too low to draw firm conclusions. Highest SUV_{max} occurred in a patient with anaplastic thyroid cancer with tumor PD-L1 expression of 90%, who experienced a partial response. Recent studies of patients with anaplastic thyroid cancer suggest that molecular-based personalized therapies, including PD-L1 antibody treatment, show improvements in survival (21, 22).

At the 10-mg ^{89}Zr-CX-072 dose, we had the opportunity to compare the results of PET imaging with 10 mg of the ^{89}Zr-labeled PD-L1 antibody atezolizumab (8). At that dose, ^{89}Zr-CX-072 uptake in the bone marrow and lymph nodes was indeed lower than ^{89}Zr-atezolizumab. Remarkably, after initial significant ^{89}Zr-CX-072 uptake in the spleen on day 2, no further increase occurred through day 7. This ^{89}Zr-CX-072 spleen uptake was similar to ^{89}Zr-atezolizumab at 1 hour after injection. However, ^{89}Zr-atezolizumab spleen uptake increased subsequently. PD-L1 is expressed in the spleen by immune cells but also by littoral cells that line the splenic sinuses of the red pulp. High perfusion of the spleen is the primary filter for the blood (23, 24). Therefore, the rapid high uptake of ^{89}Zr-CX-072, already on day 2 post-injection, may well be explained by specific binding of ^{89}Zr-CX-072 to PD-L1 expressing littoral cells.

The affinity of CX-072 to PD-L1 (K_D = 9.9 nmol/L) is lower compared with atezolizumab (K_D = ~0.30 nmol/L) when masked and similar when activated (K_D = 0.25 nmol/L; ref. 10). So, even in its

masked form, CX-072 still has measurable, although low, affinity for PD-L1, which could result in PD-L1 binding without protease cleavage of the linker and mask.

Interestingly, spleen uptake decreased when protein dose supplementation of CX-072 as part of the tracer increased. This phenomenon was not studied with ^{89}Zr-atezolizumab PET imaging, as only a 10-mg dose was applied, but it was also reported for the labeled PD-L1 antibody ^{89}Zr-durvalumab (25). Therefore, the rapid high uptake, already on day 2 post-injection, likely by binding of ^{89}Zr-CX-072 to PD-L1 expressing littoral cells, is rapidly partly saturated by higher protein doses. The same saturation did not occur in other healthy tissues.

For other lymphoid tissues, for example, bone marrow ^{89}Zr-CX-072 quantitative uptake was approximately half as much compared with the ^{89}Zr-atezolizumab PET imaging study. Uptake of ^{89}Zr-CX-072 in nonmalignant lymph nodes and of ^{89}Zr-atezolizumab was scored the same way. Visual uptake of lymph nodes in the ^{89}Zr-CX-072 study was ∼20% lower for axillary and inguinal stations compared with ^{89}Zr-atezolizumab PET imaging study. Uptake in other healthy tissues was comparable with uptake seen with other antibodies, namely, low uptake in the brain, lung, cortical bone, muscle, a subcutaneous tissue, and higher uptake in liver, kidney, and intestine, reflecting antibody metabolism and elimination (9, 15, 16).

Although procedures, equipment, and reconstruction protocol were uniform, results comparing ^{89}Zr-CX-072 with ^{89}Zr-atezolizumab should be interpreted cautiously, as the current study was not a head-to-head comparison of the two antibodies. However, a comparison of the kinetics of both tracers shows ^{89}Zr-CX-072 has similar kinetics of nonspecific uptake in normal tissues, similar kinetics of specific uptake in tumor lesions, and less specific uptake in organs with the target outside the tumor microenvironment.

This is the first report of imaging in humans using a ^{89}Zr-labeled Probody therapeutic that is conditionally activated in the tumor microenvironment. The findings of accumulation in the tumor, and modest uptake in normal lymphoid organs, support tumor-associated protease cleavage of the mask with subsequent target engagement in the tumor and decreased target engagement outside the tumor. Taking together, our findings suggest that already significant insight into the whole-body distribution of a new specialized designed medicine can be reached with a small number of patient subjects.

Authors' Disclosures

M.N. Lub-de Hooge reports conflict of interest related to CytomX-UMCG. A.H. Brouwers reports grants from CytomX Therapeutics, Inc. and nonfinancial support from CytomX Therapeutics, Inc. during the conduct of the study. M.T.L. Nguyen is a full-time employee of CytomX Therapeutics, Inc. H. Lu is a full-time employee of CytomX Therapeutics, Inc. J.A. Gietema reports grants from Roche, AbbVie, and Siemens during the conduct of the study. D.J.A. de Groot reports grants from CytomX Therapeutics, Inc. during the conduct of the study. O. Vasiljeva is a full-time employee of CytomX Therapeutics, Inc. E.G.E. de Vries reports grants from CytomX Therapeutics, Inc. during the conduct of the study, as well as other support from Daiichi Sankyo, NSABP, and Crescendo Biologics, and grants from Amgen, Bayer, Crescendo Biologics, G1 Therapeutics, Genentech, Regeneron, Roche, Servier, and Synthon outside the submitted work. No disclosures were reported by the other authors.

Authors' Contributions

L. Kist de Ruijter: Writing–original draft, writing–review and editing, acquisition of data (acquired and managed patients, etc.), analysis and interpretation of data. **J.S. Hooiveld-Noeken:** Writing–review and editing, acquisition of data (acquired and managed patients, etc.). **D. Giesen:** Writing–review and editing, acquisition of data. **M.N. Lub-de Hooge:** Conceptualization, writing–review and editing, acquisition of data. **I.C. Kok:** Writing–review and editing, acquisition of data (acquired and managed patients, etc.). **A.H. Brouwers:** Methodology, writing–review and editing, image interpretation. **S.G. Elias:** Data curation, formal analysis, visualization, writing–review and editing, analysis and interpretation of data (statistical analysis, biostatistics, computational analysis). **M.T.L. Nguyen:** Methodology, writing–review and editing. **H. Lu:** Data curation, methodology, writing–review and editing. **J.A. Gietema:** Writing–review and editing, acquisition of data (acquired and managed patients, etc.). **M. Jalving:** Writing–review and editing, acquisition of data (acquired and managed patients, etc.). **D.J.A. de Groot:** Conceptualization, formal analysis, writing–review and editing, acquisition of data (acquired and managed patients, etc.). **O. Vasiljeva:** Conceptualization, data curation, writing–review and editing. **E.G.E. de Vries:** Conceptualization, data curation, writing–original draft, writing–review and editing.

Acknowledgments

We thank Dr. R. Boellaard for support PET analyses. S. Davur, E. Ureno, and S. Viswanathan (CytomX Therapeutics, Inc.) assisted with producing and characterizing clinical-grade ^{89}Zr-CX-072. We thank the Clinical Development team of CytomX Therapeutics, Inc. (especially V. Huels, M. Will, and S. Yalamanchili) for the support of substudy design and execution. A research grant of CytomX Therapeutics, Inc. supported this study to the UMCG, Groningen, the Netherlands. The study drug CX-072 and control molecules were supplied by CytomX Therapeutics, Inc. (PROBODY is a U.S. registered trademark of CytomX Therapeutics, Inc.).

The costs of publication of this article were defrayed in part by the payment of page charges. This article must therefore be hereby marked *advertisement* in accordance with 18 U.S.C. Section 1734 solely to indicate this fact.

Received February 17, 2021; revised April 24, 2021; accepted July 9, 2021; published first July 12, 2021.

References

1. Hodi FS, Chesney J, Pavlick AC, Robert C, Grossmann KF, McDermott DF, et al. Combined nivolumab and ipilimumab versus ipilimumab alone in patients with advanced melanoma: 2-year overall survival outcomes in a multicentre, randomised, controlled, phase 2 trial. Lancet Oncol 2016;17:1558–68.
2. Motzer RJ, Rini BI, McDermott DF, Frontera OA, Hammers HJ, Carducci MA, et al. Nivolumab plus ipilimumab versus sunitinib in first-line treatment for advanced renal cell carcinoma: extended follow-up of efficacy and safety results from a randomised, controlled, phase 3 trial. Lancet Oncol 2019;20:1370–85.
3. Hellmann MD, Paz-Arez L, Bernabe Caro R, Zurawski B, Kim SW, Costa EC, et al. Nivolumab plus ipilimumab in advanced non–small-cell lung cancer. N Engl J Med 2019;381:2020–31.
4. Martins F, Sofiya L, Sykiotis GP, Lamine F, Maillard M, Fraga M, et al. Adverse effects of immune-checkpoint inhibitors: epidemiology, management and surveillance. Nat Rev Clin Oncol 2019;16:563–80.
5. de Vries EGE, de Ruijter LK, Lub-de Hooge MN, Dierckx RA, Elias SG, Oosting SF. Integrating molecular nuclear imaging in clinical research to improve anticancer therapy. Nat Rev Clin Oncol 2019;16:241–55.
6. van de Donk PP, Ruijter LK, Lub-de Hooge MN, Brouwers AH, van der Wekken Oosting SF, et al. Molecular imaging biomarkers for immune checkpoint inhibitor therapy. Theranostics 2020;10:1708–18.
7. Waaijer SJH, Kok IC, Eisses B, Schröder CP, Jalving M, Brouwers AH, et al. Molecular imaging in cancer drug development. J Nucl Med 2018;59:726–32.
8. Bensch F, van der Veen EL, Lub-de Hooge MN, Jorritsma-Smit A, Boellaard R, Kok IC, et al. 89Zr-atezolizumab imaging as a non-invasive approach to assess clinical response to PD-L1 blockade in cancer. Nat Med 2018:24;1852–8.
9. Gebhart G, Lamberts LE, Wimana Z, Garcia C, Emonts P, Ameye L, et al. Molecular imaging as a tool to investigate heterogeneity of advanced

HER2-positive breast cancer and to predict patient outcome under trastuzumab emtansine (T-DM1): the ZEPHIR trial. Ann Oncol 2016;27: 619–24.
10. Giesen D, Broer LN, Lub-de Hooge MN, Popova I, Howng B, Nguyen M, et al. Probody therapeutic design of ^{89}Zr-CX-072 promotes accumulation in PD-L1-expressing tumors compared to normal murine lymphoid tissue. Clin Cancer Res 2020;26:3999–4009.
11. Naing A, Thistlethwaite F, de Vries EGE, Eskens FALM, Uboha N, Ott PA, et al. CX-072 (Pacmilimab), a probody® PD-L1 inhibitor in advanced or recurrent solid tumors (PROCLAIM-CX-072): an open-label dose-finding and first-in-human study. J Immunother Cancer 2021; in press.
12. Sanborn RE, Hamid O, de Vries EGE, Ott PA, Garcia-Corbacho J, Boni V, et al. CX-072 (Pacmilimab), a Probody® PD-L1 inhibitor, in combination with ipilimumab in subjects with advanced solid tumors (PROCLAIM-CX-072): a first-in-human, dose-finding study. J Immunother Cancer 2021; in press.
13. Eisenhauer EA, Therasse P, Bogaerts J, Schwartz LH, Sargent D, Ford R, et al. New response evaluation criteria in solid tumours: revised RECIST guideline (version 1.1). Eur J Cancer 2009;45:228–47.
14. Bohnsack O, Hoos A, Ludajic K. Adaptation of the immune related response criteria: irRECIST. Ann Oncol 2014;25:iv361–iv372.
15. Lamberts TE, Menke-van der Houven van Oordt CW, ter Weele EJ, Bensch F, Smeenk MM, et al. ImmunoPET with anti-mesothelin antibody in patients with pancreatic and ovarian cancer before anti-mesothelin antibody-drug conjugate treatment. Clin Cancer Res 2016;22:1642–52.
16. Bensch F, Brouwers AH, Lub-de Hooge MN, de Jong JR, van der Vegt B, Sleijfer S, et al. 89Zr-trastuzumab PET supports clinical decision making in breast cancer patients, when HER2 status cannot be determined by standard work up. Eur J Nucl Med Mol Imaging 2018;45;2300–6.
17. Makris NE, Boellaard R, Visser EP, de Jong JR, Vanderlinden B, Wierts R, et al. Multicenter harmonization of ^{89}Zr PET/CT performance. J Nucl Med 2014;55; 264–7.
18. Boellaard R. Quantitative oncology molecular analysis suite: ACCURATE. J Nucl Med 2018;59: (Suppl; Abstr 1753).
19. Stroh M, Green M, Miljard BL, Apgar JF, Burke JM, Garner W, et al. Model-informed drug development of the masked antiPDL1 antibody CX-072. Clin Pharmacol Ther 2021;109:383–93.
20. Doroshow DB, Bhalla S, Beasley MB, Sholl LM, Kerr KM, Gnjatic S, et al. PD-L1 as a biomarker of response to immune-checkpoint inhibitors. Nat Rev Clin Oncol 2021;12. doi: 10.1038/s41571–021–00473–5. Epub ahead of print.
21. Maniakas A, Dadu R, Busaidy NL, Wang JR, Ferrarotto R, Lu C, et al. Evaluation of overall survival in patients with anaplastic thyroid carcinoma, 2000–2019. JAMA Oncol 2020;6:1397–404.
22. Capdevila J, Wirth LJ, Ernst T, Aix SP, Lin CC, Ramlau R, et al. PD-1 blockade in anaplastic thyroid carcinoma. J Clin Oncol 2020;38:2620–7.
23. Bronte V, Pittet M. The spleen in local and systemic regulation of immunity. Immunity 2013;39:806–18.
24. Cataldi M, Vigliotti C, Mosca T, Cammarota MR, Capone D. Emerging role of the spleen in the pharmacokinetics of monoclonal antibodies, nanoparticles and exosomes. Int J Mol Sci 2017;18:1249.
25. Verhoeff S, van de Donk PP, Aarntzen EHJG, Miedema IHC, Oosting SF, Voortman J, et al. 89Zr-durvalumab PD-L1 PET in recurrent or metastatic (R/M) squamous cell carcinoma of the head and neck. J Clin Oncol 2020:38 (Suppl; Abstr 3573).

Published OnlineFirst July 12, 2021; DOI: 10.1158/1078-0432.CCR-21-0453

Clinical Cancer Research

First-in-Human Study of the Biodistribution and Pharmacokinetics of ^{89}Zr-CX-072, a Novel Immunopet Tracer Based on an Anti–PD-L1 Probody

Laura Kist de Ruijter, Jahlisa S. Hooiveld-Noeken, Danique Giesen, et al.

Clin Cancer Res 2021;27:5325-5333. Published OnlineFirst July 12, 2021.